Journal of Inorganic and Organometallic Polymers and Materials
https://doi.org/10.1007/s10904-025-04117-4

RESEARCH

Zr-Functionalized Polysulfone Hybrids for Arsenite and Arsenate Removal from Aqueous Media

A. V. Montella[1] · M. Bastianini[2] · M. Sisani[2] · I. Ahmed[1] · E. Sgreccia[1] · M. L. Di Vona[1] · R. Narducci[1]

Received: 24 September 2025 / Accepted: 14 November 2025

Abstract
Hybrid polymers based on polysulfone (PSU), covalently functionalized with zirconium-organic moieties, were developed and applied for arsenic removal from wastewater. The synthesis strategy involved anchoring a terephthalate moiety onto PSU to act as a metal–organic framework (MOF) linker, followed by MOF assembly and subsequent quaternization (QA) with trimethylamine (TMA). The covalent incorporation of MOF-like units within the polymer backbone effectively minimized the risk of leaching; indeed, Zr release under highly basic conditions was measured at less than 1% of the total Zr content. Two materials, Zr-PSU and Zr-PSU-QA, were synthesized, characterized, and tested for As(III) and As(V) adsorption. The adsorption efficiency was assessed using ICP analysis at different pH values (3, 7, and 12) to account for variations in the charge of the Zr-organic moieties and the speciation of arsenic. Two arsenic concentrations (0.5 and 1 mM) were investigated. The results demonstrated that Zr-PSU at pH = 3 achieved a removal efficiency (RE%) of 77% for As(V), attributed to the positively charged Zr-framework at this pH. At neutral pH, significant As(III) adsorption was also observed. Additionally, Zr-PSU-QA at pH = 12 exhibited an RE% of 35% for As(III) due to the positively charged ammonium moieties in the polymer matrix. Kinetic studies for Zr-PSU at pH = 3 (As(V)) showed a plateau within 8 h, fitting a pseudo-second-order model. Regeneration with NaCl enabled partial recovery, which increased to 98.9% after four cycles when the hybrid material was supported on glass beads (GBs). Compared with previously reported Zr–MOF/polymer composites, this covalently integrated system exhibits enhanced structural stability, low leaching, and combined adsorption–ion exchange functionality. The results demonstrate the potential of Zr-PSU and Zr-PSU-QA as robust, regenerable materials for heavy-metal removal and their suitability for integration into flow-through water treatment systems.

Keywords MOF-like structures · Porous organic polymers · Quaternary ammonium · Regeneration efficiency · Wastewater decontamination

1 Introduction

The growing demand for safe drinking water, driven by population growth and industrial development, has been paralleled by an alarming increase in heavy metals in wastewater [1]. The presence of different toxic, carcinogenic heavy metals in the effluents makes their recycling very difficult and their removal has become a crucial process [2, 3]. Among them, arsenic is particularly concerning due to its high toxicity and cocarcinogenic effects on human organs such as lung, liver, kidney, and bladder [4]. The World Health Organization (WHO) has set a provisional guideline of 10 μg L^{-1} for arsenic in drinking water, yet much higher concentrations are often detected. For instance, in the Viterbo area (Italy), levels reach 75 μg L^{-1} at Fabrica di Roma and 52 μg L^{-1} in Bagnoregio (UNESCO site) [5]. Arsenic occurs in different oxidation states, most commonly as As(III) (arsenite) and As(V) (arsenate). Under oxidizing conditions, As(V) predominates, while As(III) prevails in reducing environments [6]. The removal of arsenic from water is therefore a critical challenge. Traditional methods such as ion exchange, adsorption, membrane separation, and precipitation are widely investigated but often face

✉ R. Narducci
riccardo.narducci@uniroma2.it

[1] Dep. Industrial Engineering and International Laboratory: Ionomer Materials for Energy, Tor Vergata University of Rome, Via del Politecnico 1, 00133 Roma, Italy

[2] Prolabin & Tefarm s.r.l., Via dell'Acciaio 9, 06134 Perugia, Italy

Published online: 03 December 2025

significant drawbacks, including cost constraints and poor regeneration [7]. Metal − organic frameworks (MOFs), higly porous materials formed by inorganic metal nodes connected by organic ligands, have attracted strong interest as adsorbents thanks to their excellent tunability and well-ordered structure. MOFs have been applied in catalysis [8–10] gas separation [11–14], and water purification, including arsenic adsorption [15–17]. UiO-66, a Zr-based MOF, has been particularly studied for its exceptional stability and high affinity toward arsenic species, attributed to electrostatic interactions, Zr–O–As coordination, and chelation effects [18]. Two binding sites have been proposed for arsenic species within the framework: hydroxyl groups and benzenedicarboxylate ligands, allowing multiple arsenic species to coordinate with each Zr cluster [19–21]. Nevertheless, the practical use of MOFs in water treatment applications remains limited by their cost, poor processability, and challenges in recovery and reuse [18, 22].

Recent strategies to overcome the limitations of conventional MOFs focus on their integration with polymers [23]. Hybrid MOF–polymer composites combine the ordered porosity and high adsorption capacity of MOFs with the mechanical strength, stability, and processability of polymers. Unlike previous studies relying on physical mixtures or surface coatings, this work employs a covalent integration strategy, which enhances robustness, prevents particle detachment, and improves long-term aqueous stability. The covalent linkage promotes homogeneous dispersion of MOF units, minimizes leaching, and induces intrinsic porosity in the polymer, forming a porous organic polymer (POP) with abundant active sites [24, 25]. The resulting materials can be readily processed into membranes, beads, or films, offering versatility for various water treatment applications. Additionally, the polymer framework can be functionalized with specific groups, such as quaternary ammonium moieties, that enhance arsenic binding and complement the adsorption capability of the MOF structure.

Different strategies for covalent MOF–polymer connections have been reported, including "polymerization of the framework," where organic ligands simultaneously serve as both MOF linkers and polymer chains [26–28]. Covalently linked MOF-polymer composites have been successfully applied in various fields including fuel cells [14], CO_2 separation [29, 30], and stimulus-responsive heterogeneous catalysis [31, 32].

In our previous work we explored the ability of covalently bonded hybrid polymers to MOF-like structures as catalytic electrodes [33]. In this study, polysulfone (PSU) was chosen as the polymer matrix due to its availability, low cost, and ease of functionalization. Terephthalate ligands were grafted onto PSU to serve as linkers for the assembly of a Zr-MOF-like framework, generating Zr-PSU. Subsequent functionalization with quaternary ammonium (QA) groups produced Zr-PSU-QA, an anion-exchange hybrid polymer. These materials integrate three key functionalities: porosity from the MOF-like domains, adsorption activity from Zr centers, and additional binding sites from QA groups. The resulting hybrid polymers were thoroughly characterized and tested for the removal of arsenite and arsenate across a range of pH values and concentrations. Experiments evaluated both powdered forms and coatings on glass beads (GBs), facilitating integration into flow-through cartridge systems. Regeneration tests showed that while simple NaCl treatment provided partial recovery, GB-supported materials achieved 98.9% regeneration efficiency after four cycles. These results, combined with material stability and compatibility with cartridge operation, demonstrate that Zr-PSU and Zr-PSU-QA are promising candidates for practical, scalable arsenic removal from wastewater, with further optimization potential.

2 Experimental Section

2.1 Materials

Polysulfone UDEL P-1800 NT11 (PSU), terephthalic acid 98% (1,4-BDC), diethyl 2,5-dihydroxyterephthalate 97%, trimethylamine (TMA, 4.2 M in ethanol), 1-methyl-2-pyrrolidone (NMP), dimethyl sulfoxide (DMSO), *N*, *N*-dimethylformamide (DMF), chloroform ($CHCl_3$), $ZrCl_4$ 99.5%, As_2O_3 ACS reagent, $Na_2HAsO_4{*}7H_2O \geq 98\%$, NaOH 98%, Glass beads 1 mm, and other chemicals were used as received from Sigma-Aldrich without further purification.

2.2 Synthesis

2.2.1 PSU-Precursor

PSU-CH_2Cl was obtained by the procedure already described [34]. Two separate solutions were prepared [33]. (A) 2.0 g (3.8 mmol) of PSU-CH_2Cl (1.7 degree of chloromethylation, DCM) were dissolved in 50 mL of anhydrous DMF under N_2 flux at 50 °C, then 0.10 g of KI (0.64 mmol) were added under stirring. (B) in 20 mL of anhydrous DMF were dissolved 0.82 g (3.2 mmol) of diethyl 2,5-dihydroxyterephthalate (in molar ratio 0.5 with respect to the chloromethyl groups) and 0.45 g, (3.2 mmol) of K_2CO_3. The mixture was heated overnight at 80 °C under nitrogen flux. The A and B solutions were combined and reacted at 70 °C for 72 h. The solution was then treated with 10wt% of NaOH in 50:50 H_2O/MeOH at 60 °C for 2 h to hydrolyze the residual esters. To obtain the H-form, the solution was precipitated with 30 mL of 2 M HCl and 30 mL of ethanol

and digested overnight. The PSU-precursor was filtered and washed several times with water/ethanol and stored on P_2O_5 at RT. Yield = 75%.

2.2.2 Zr-PSU

(A) In 40 mL of anhydrous DMF, 1.0 g (1.74 mmol) of PSU-precursor was dissolved under N_2 flux and 0.250 g (1.5 mmol) of terephthalic acid were added and mixed for 30 min. (B) In 10 mL of anhydrous DMF, were added 0.1 mL of double distilled water and 0.4 g of $ZrCl_4$ (1.5 mmol) and stirred for 30 min. The two solutions were mixed for 30 min, placed in a Teflon bottle and put in the oven for 16 h at 120 °C. The product was washed with HCl 0.1 N and acetone 3 times and stored on P_2O_5. Yield = 100%. The percentage of Zr estimated by XPS was 1.4 atom% [33].

2.2.3 Zr-PSU-QA

0.8 g (1.2 mmol) of Zr-PSU were dissolved overnight under N_2 flux in NMP, then 0.48 mL of TMA (2.0 mmol) were added and left to react at 80 °C for 3 days under stirring. The product was dried under high vacuum and washed with H_2O and dried again [34]. The degree of amination, estimated by NMR, was 1.15.

2.2.4 Glass Beads (GBs) Coated with Zr-PSU

Glass beads (1 mm diameter) were coated with PSU or a PSU/Zr-PSU mixture following the method described in [35]. For all coatings, the active material (Zr-PSU) was maintained at 10 mg. PSU was included to improve adhesion of the polymer to the GB surface. Coated GBs were subsequently tested in As(V) adsorption and regeneration experiments and intended for integration into flow-through cartridges.

Blank GBs (PSU only): 150 mg of GBs were combined with 15 mg PSU dissolved in 10 mL $CHCl_3$. The solvent was evaporated at 90 °C over 24 h.

GBs with PSU/Zr-PSU: 150 mg of GBs were coated with a solution of 15 mg PSU and 10 mg Zr-PSU in 10 mL $CHCl_3$. The solvent was evaporated at 90 °C over 24 h, yielding uniformly coated GBs suitable for adsorption and regeneration studies.

2.3 Batch Adsorption Studies

Appropriate amounts of As_2O_3 and $Na_2HAsO_4 \cdot 7\ H_2O$ were dissolved in double-distilled water to prepare As(III) and As(V) solutions at 0.5 and 1 mM. Samples containing 10 ± 0.3 mg of Zr-PSU or Zr-PSU-QA powders were prepared. The pH of each solution was adjusted according to Table 1 using 37wt% HCl or 1 M NaOH. As(III) solutions at pH = 12 were prepared under a nitrogen atmosphere to prevent OH^- carbonation.

For adsorption experiments, the Zr-PSU and Zr-PSU-QA powders were added to the prepared arsenic solutions. The mixtures were stirred in closed vessels at room temperature for 24 h. After adsorption, the suspensions were filtered using polyamide membrane filters (0.2 µm pore size, Whatman) prior to further analysis.

The removal efficiency (RE%) and the adsorption capacity (q, mg/g) of each system was evaluated using the formula:

$$RE\,(\%) = \frac{c_0 - c}{c_0} \cdot 100 \tag{1}$$

$$q = \frac{c_0 - c}{m} \cdot V \tag{2}$$

Where c_0 and c are the concentration, before and after sorption, m the absorbent mass and V of treated solution.

Table 1 Results of as (V) and (III) uptake by Zr-PSU and Zr-PSU-QA. The quantity of the sample added for each batch (15 mL) was 10 ± 0.3 mg

System	Metal	Sample	pH/ [As] mM	RE %	q (mg/g)	mg As per mg Zr[a)]
a	As (V)	Zr-PSU-QA	3/[0.5]	31.1	17.0	267.5
b	As (V)	Zr-PSU-QA	3/[1.0]	25.4	28.5	448.5
c	As (V)	Zr-PSU	3/[0.5]	77.0	43.3	681.4
c'	As (V)	GB/PSU	3/[0.5]	0.3	0.17	2.6
c''	As (V)	GB/PSU + Zr-PSU	3/[0.5]	62.5[b)]	35.1	552.3
d	As (V)	Zr-PSU	3/[1.0]	58.9	66.2	1041.7
e	As (V)	Zr-PSU-QA	12/[0.5]	5.2	2.97	46.7
f	As (V)	Zr-PSU-QA	12/[1.0]	9.9	11.0	173.1
g	As (III)	Zr-PSU	7/[0.5]	27.2	15.2	239.2
h	As (III)	Zr-PSU	7/[1.0]	35.5	39.9	627.9
i	As (III)	Zr-PSU-QA	12/[0.5]	34.5	19.4	305.3

a Normalized adsorption (based on Zr = 63.55 ppm); **b** Considering only the active material (e.g. Zr-PSU, see below)

2.3.1 Stability of Zr-PSU and Zr-PSU-QA

The chemical stability of the hybrid materials was evaluated by monitoring zirconium release under different pH conditions. Samples of Zr-PSU and Zr-PSU-QA (10 mg) were immersed in 10 mL of aqueous solutions adjusted to pH 3, 7, and 12, respectively, and maintained under stirring at room temperature. Aliquots were collected after 1 h, 2 h, 16 h, and 24 h, filtered, and analyzed by ICP-OES to determine the Zr concentration in solution. For Zr-PSU, the Zr concentrations were 0.043 ppm (1 h) and 0.044 ppm (24 h) at both pH 3 and 7, while at pH 12, the Zr concentration after 24 h reached 0.51 ppm. For Zr-PSU-QA, the Zr concentrations at pH 12 were 0.044 ppm (1 h), 0.055 ppm (2 h), 0.081 ppm (16 h), and 0.084 ppm (48 h). Considering the total Zr content of 63.55 ppm (determined after complete digestion in 25 M NaOH at 80 °C for 96 h and in agreement with XPS results [33]), these values correspond to less than 1% Zr leaching even under strongly basic conditions, confirming the high stability of the covalently linked hybrid systems in aqueous environments.

2.3.2 Kinetic Measurements

The kinetic measurements were performed for the sample Zr-POP at pH = 3 (0.5 mM, As(V)), at 30 min, 1, 2, 4, 8, 16, and 24 h of immersion.

2.3.3 Regeneration

The Zr-PSU sample was chosen for the regeneration tests. The system was placed at pH = 3 in 0.5 mM As(V); after 24 h the powder was filtered and regenerated with 1 M NaCl solution overnight. The material was then filtered and washed with dd water several times, dried over P_2O_5 and weighted. The renewed sample was inserted again into the same volume of fresh As(V) solution. Regeneration was performed for 3 cycles. The same procedure was used with PSU/Zr-PSU-coated GBs. Regeneration was performed for 4 cycles.

2.4 Characterization Techniques

2.4.1 Ion Exchange Capacity

The IEC (milliequivalents per gram of dry polymer) was determined by potentiometric acid–base titration. For OH^- form, the finely ground powder of Zr-PSU-QA was treated in NaOH 0.1 M solution for 24 h and washed with bidistilled water to remove the excess of NaOH for 48 h. After drying for 3 days over P_2O_5, the powder was weighed and immersed in 0.02 M HCl for 2 days. The acid solution was then back-titrated with 0.02 M NaOH. The IEC was 1.93 meq/g.

2.4.2 ^{1}H-NMR Spectroscopy

^{1}H-NMR spectra were recorded with a Bruker Avance 700 spectrometer operating at 700.18 MHz using deuterating solvents (DMSO-d_6, $CDCl_3$). A small portion of synthesized materials were treated under vacuum before NMR analysis.

2.4.3 FTIR Spectroscopy

FTIR spectra were recorded in transmission mode in the range of 4000–500 cm^{-1} using a Perkin Elmer Spectrum 2 IR spectrometer equipped with an ATR Zinc Selenide (ZnSe) crystals.

2.4.4 Inductively Coupled Plasma–Optical Emission Spectroscopy (ICP-OES)

The heavy metal ion concentrations were determined by ICP-OES Perkin Elmer, Avio 200. The solutions were analyzed after a proper dilution.

2.4.5 2.4.5. Brunauer-Emmett-Teller (BET) Analysis

The BET surface area was determined via nitrogen gas sorption at 77 K. The samples were vacuum-degassed at 250 °C before the analysis. The BET surface area of Zr-PSU was 269 m^2/g and for Zr-PSU-QA 192.5 m^2/g.

2.4.6 X-ray Diffraction (XRD) Analysis

XRD patterns were collected using a Panalytical X'Pert PRO diffractometer with CuKα radiation, a step size of 0.033°, and a step scan of 50 s. The XRD diffractograms show an amorphous pattern for both samples.

3 Results and Discussion

The synthesis routes of PSU-precursor, Zr-PSU, and Zr-PSU-QA are illustrated in Fig. 1. Chloromethyl groups present in polysulfone (DCM = 1.7) were reacted with phenolate groups of terephthalic ester via an S_N2 reaction. As detailed in the Experimental section, the stoichiometry was carefully controlled to ensure that only a fraction of the -CH_2Cl groups reacted with the phenolate. This approach leaves a portion of the chloromethyl groups unreacted, making them available for a subsequent quaternization reaction. The PSU linked with the synthon molecule was used to assemble the MOF by reaction with further terephthalic acid

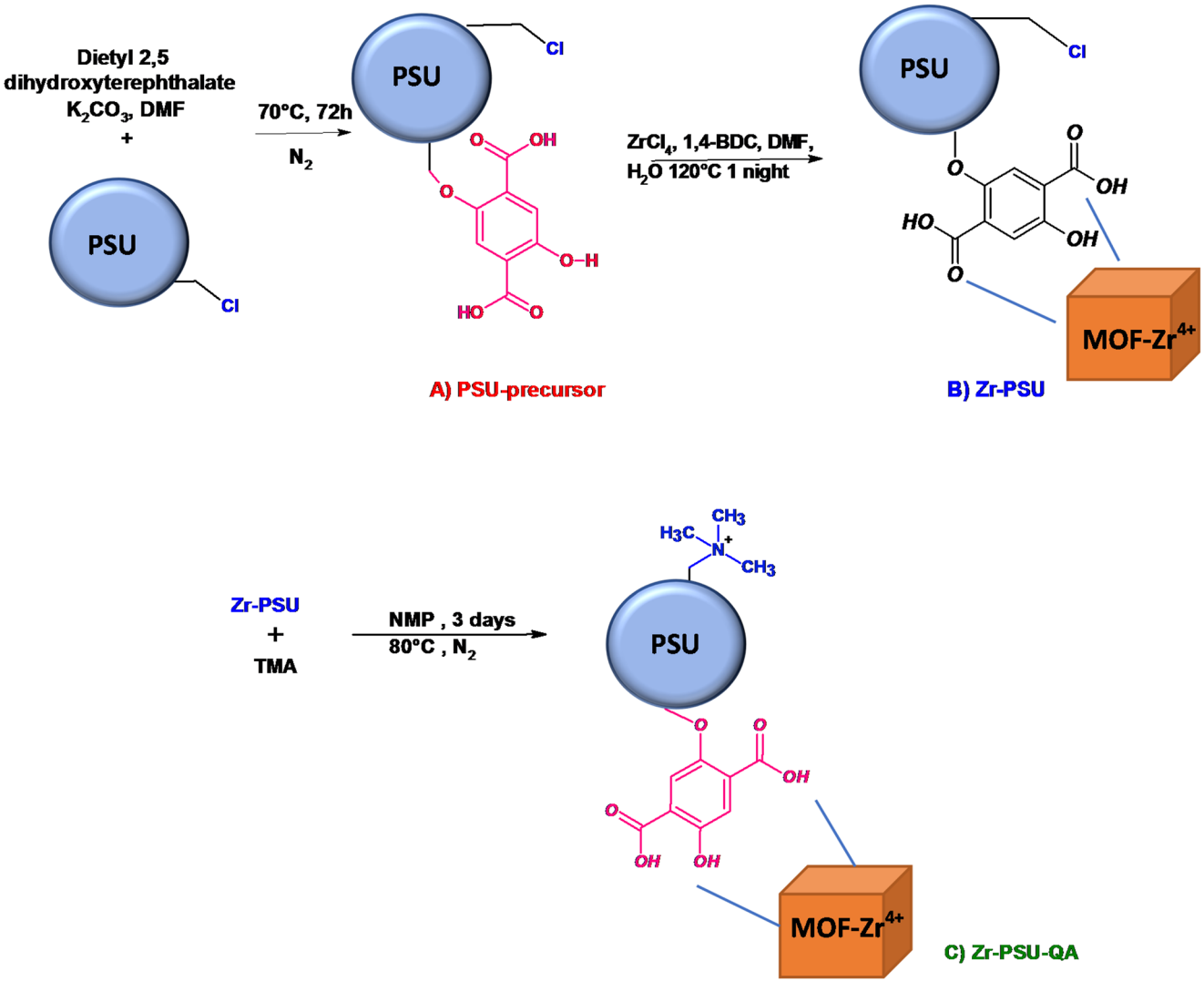

Fig. 1 Reaction sequence of the synthesis of: **A** PSU-precursor, **B** Zr-PSU, **C** Zr-PSU-QA

via solvothermal method, adapting the procedure used in the synthesis of UiO-66 [13]. The quaternization of unreacted CH_2Cl groups was carried out in the presence of TMA.

The ^{1}H-NMR spectra of PSU-precursor, Zr-PSU, and Zr-PSU-QA are shown in Fig. 2, despite their low solubility, particularly for the Zr-PSU sample. All spectra exhibit characteristic signals of PSU, including the aromatic region (6.7–8.1 ppm) and the two methyl groups linked to the quaternary carbon at 1.6 ppm. The signals corresponding to the ether bond between the phenolic group of terephthalic ester and the chloromethyl groups of PSU appear as a split peak between 5.30 and 5.42 ppm (Fig. 2a), reflecting the reaction occurring at two distinct chloromethyl groups. The residual chloromethyl groups are observed at 4.4 ppm.

Considering 6 H for the methyl groups of PSU, the ether bond integration corresponds to 0.6 H, indicating a degree of functionalization of 0.3, while the remaining chloromethyl moiety accounts for approximately 1.3 H. Upon assembly of the Zr-MOF-like structure (Fig. 2b), the peak areas and overall spectral features remain largely unchanged, apart from further splitting of the ether signal due to interaction with the metal. In the final spectrum of Zr-PSU-QA (Fig. 2c), the presence of CH_2 linked to the ammonium group is confirmed, and it is split into three peaks centered at 4.4 ppm. Additionally, the CH_3 groups attached to the ammonium appear at approximately 2.9 ppm, also showing a three-peak pattern. The ratio of the areas of the ether bonds, benzylammonium groups and methyl groups of PSU remains constant.

Figure 3 compares the FTIR spectra of PSU-precursor, Zr-PSU, and Zr-PSU-QA. In the PSU-precursor, the presence of the peak at 1730 cm^{-1} is due to the C = O stretch of terephthalic acid linked by ether bond to PSU. Other signals are due to the typical absorptions of PSU [34] and

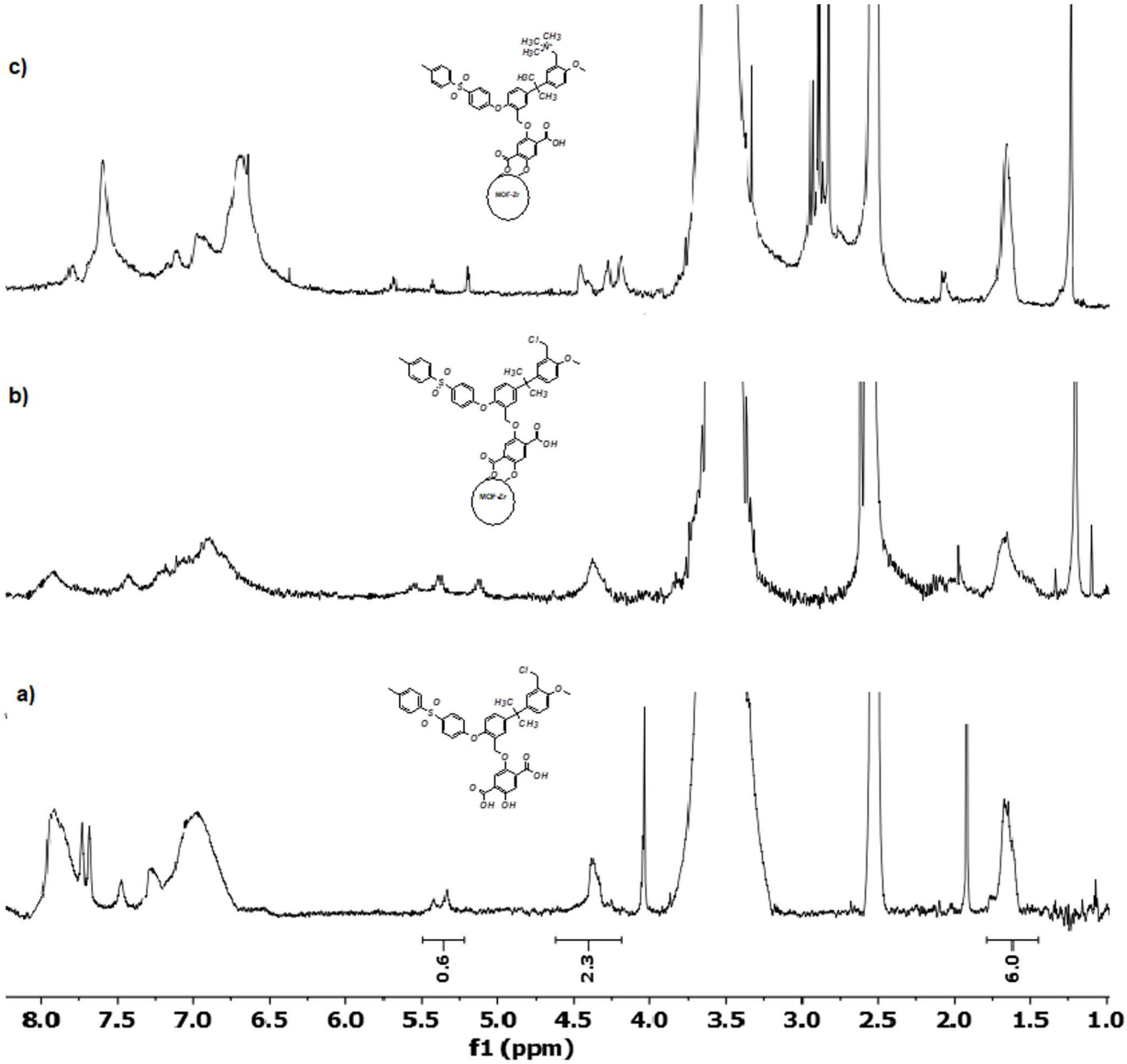

Fig. 2 ^{1}H-NMR of **a** PSU-precursor, **b** Zr-PSU, **c** Zr-PSU-QA in DMSO-d_6

terephthalic acid. For the Zr-PSU compound, the peak at 1730 cm^{-1} disappears, and the shift of the signal from 1670 cm^{-1} (carboxylate) to 1650 cm^{-1} is observed. In fact, as a result of the Zr coordination, carboxylates present two peaks, asym and sym stretches at 1650 and 1400 cm^{-1}, respectively [36]. The peaks at 750 and 650 cm^{-1} belong to Zr—O bonds [37]. The methyl groups linked to nitrogen ion ($-N^{+}Me_3$) overlap with the methyl groups of PSU [38].

XRD patterns of both Zr-PSU and Zr-PSU-QA show broad amorphous halos without distinct Bragg peaks. Although MOFs are typically crystalline, the low MOF loading (≈0.3 unit per PSU repeat unit) and covalent integration within the amorphous polysulfone matrix hinder long-range order, resulting in uniformly dispersed, short-range Zr–carboxylate domains below the XRD detection limit.

Arsenate exists in several forms, such as H_3AsO_4, $H_2AsO_4^-$, $HAsO_4^{2-}$, and AsO_4^{3-}. $H_2AsO_4^-$ is the predominant species at pH from 2 to 6, while $HAsO_4^{2-}$, AsO_4^{3-} are the main ions as pH increases from 7 to 10 [39]. As(III) exists in neutral form (H_3AsO_3) at pH < 8.0 and negatively charged ($H_2AsO_3^-$) at pH >8.0 [39, 40]. The dissociation reactions and the corresponding equilibrium constants (pKa) of H_3AsO_4 and H_3AsO_3 are shown below [41]:

As(V):

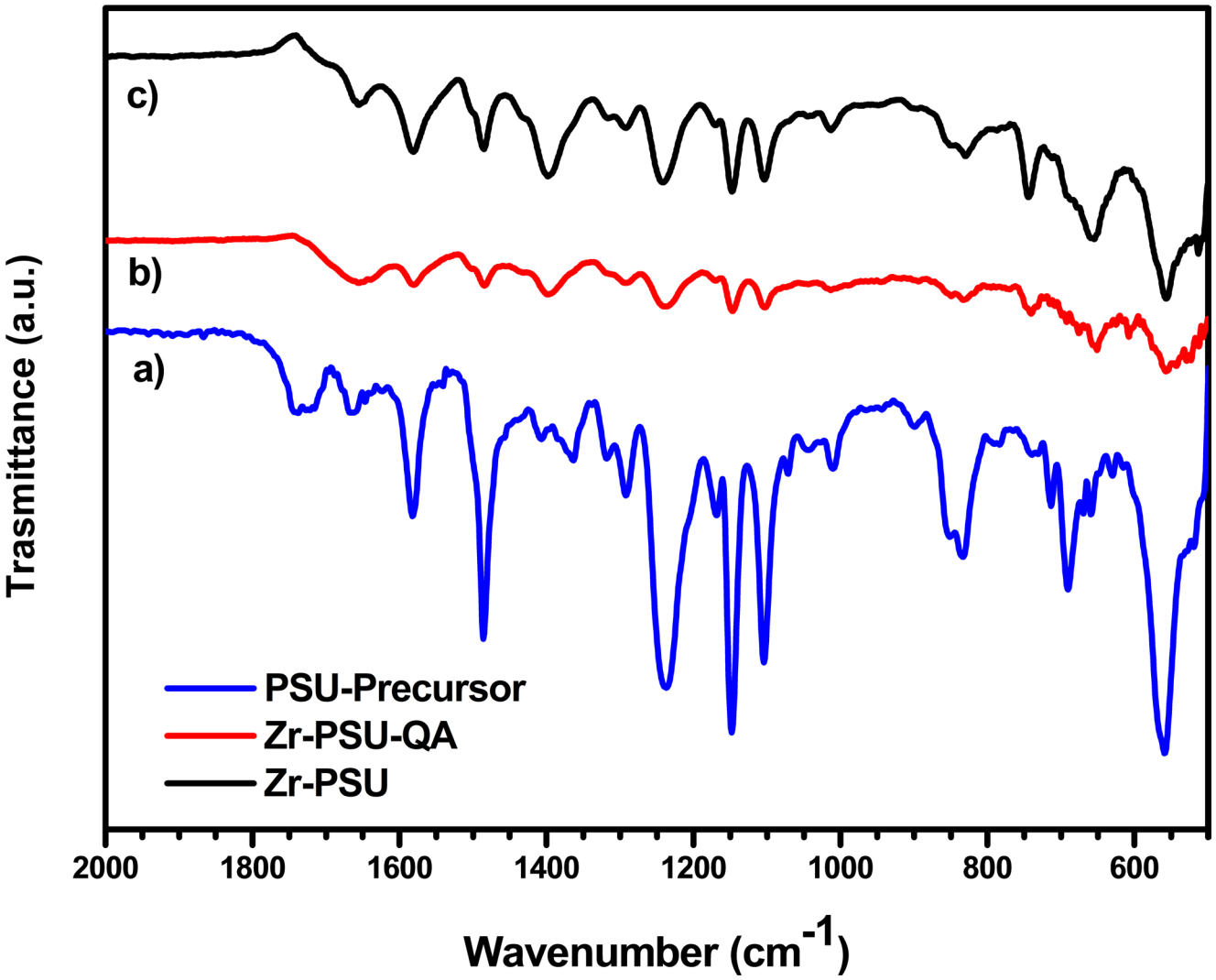

Fig. 3 FTIR spectra of **a** PSU-precursor, **b** Zr-PSU, **c** Zr-PSU-QA

$$H_3AsO_4 + H_2O \rightleftharpoons H_2AsO_4^- + H_3O^+ | pK_a = 2.24$$
$$H_3AsO_4^- + H_2O \rightleftharpoons H_2AsO_4^{2-} + H_3O^+ | pK_a = 6.69$$
$$HAsO_4^{2-} + H_2O \rightleftharpoons AsO_4^{3-} + H_3O^+ | pK_a = 11.50$$

As(III):

$$H_3AsO_3 + H_2O \rightleftharpoons H_2AsO_3^- + H_3O^+ | pK_a = 9.20$$
$$H_3AsO_3^{2-} + H_2O \rightleftharpoons H_2AsO_3^{2-} + H_3O^+ | pK_a = 12.10$$
$$HAsO_3^{2-} + H_2O \rightleftharpoons AsO_3^{3-} + H_3O^+ | pK_a = 13.40$$

Several factors influence the arsenic sorption capacity of Zr-PSU and Zr-PSU-QA systems:

Surface charge of MOF-like structures. The charge present on the MOF framework strongly affects its interaction with arsenic species. UiO-66, as reported in the literature, has a pKa of 3.52 [20], an isoelectric point (pH_{iep}) of ~ 5.5, and a point of zero charge (pH_{PZC}) of ~ 5 [42]. At pH values below 5, the MOF surface is positively charged, promoting adsorption of anionic species such as $H_2AsO_4^-$. Conversely, at pH values above 5, the surface becomes negatively charged, which can reduce electrostatic attraction depending on the oxidation state of arsenic.

Anion exchange mechanism in Zr-PSU-QA. The quaternized nitrogen groups carry a permanent positive charge, ensuring a consistently favorable Donnan effect, except for neutral arsenic species. The exchanged ion depends on the solution pH: in acidic and neutral media, chloride is exchanged, whereas under basic conditions, hydroxide becomes the primary exchanging ion:

$$HCl : \mathrm{PSU - CH_2N(CH_3)_3^+\ Cl^- + \ H_2AsO_4^-}$$
$$\rightarrow \mathrm{PSU - CH_2N(CH_3)_3^+\ H_2AsO_4^- + \ Cl^-}$$
$$NaOH : \mathrm{PSU - CH_2N(CH_3)_3^+\ OH^- + \ H_2AsO_3^-}$$
$$\rightarrow \mathrm{PSU - CH_2N(CH_3)_3^+\ H_2AsO_3^- + \ OH^-}$$

Porosity of the materials: The porosity of the hybrid materials shows a clear influence on their arsenic adsorption performance. The pristine PSU polymer, with a low surface area (6.1 $m^2\ g^{-1}$) and pore volume (0.025 $cm^3\ g^{-1}$) [43],

exhibits negligible adsorption. Incorporation of Zr–MOF-like structures markedly enhances these properties: Zr-PSU displays a BET surface area of 269 $m^2\ g^{-1}$ and a total pore volume of 0.39 $cm^3\ g^{-1}$, while Zr-PSU-QA presents slightly lower values of 192 $m^2\ g^{-1}$ and 0.30 $cm^3\ g^{-1}$, respectively [33]. The increase in average pore diameter from 5.8 nm (Zr-PSU) to 6.2 nm (Zr-PSU-QA) is attributed to the steric effects introduced by the quaternized ammonium groups. These textural improvements result in a more open network and better diffusion of arsenic species through the polymer matrix.

A quantitative comparison confirms a direct correlation between BET surface area, porosity, and adsorption capacity (q_e). At pH 3 and [As(V)] = 0.5 mM, Zr-PSU achieved 77% removal efficiency (RE%) and q_e = 43.3 mg g^{-1}, while Zr-PSU-QA, with its lower surface area and partial pore blockage, reached RE = 31.1% and q_e = 17.0 mg g^{-1}. Increasing the initial arsenic concentration to 1 mM further enhanced q_e to 66.2 mg g^{-1} for Zr-PSU, confirming that a higher porosity supports greater adsorption capacity. The GB/PSU + Zr-PSU composite maintained good performance (q_e = 35.1 mg g^{-1}) despite reduced active material content, indicating that immobilization does not hinder pore accessibility.

Table 1 shows the results for As (III) and As (V) removal in different conditions. Figure 4 shows a comparison between the data.

According to the results presented in Table 1; Fig. 4, the most efficient system for arsenic uptake was Zr-PSU (sample c) at pH = 3 with an initial concentration of 0.5 mM As (V), showing RE% = 77 and q = 43.3 mg/g. This high efficiency can be attributed to the positively charged MOF framework at acidic pH, the predominance of $H_2AsO_4^-$ species, and the enhanced porosity of the material, which together promote strong interactions with hydroxyl and carboxyl groups. Sample d exhibited a slightly lower RE but a higher adsorption capacity (q), due to the increased initial arsenic concentration.

The coated glass bead systems provided interesting insights. PSU-coated GBs (c') showed negligible adsorption, while GBs coated with PSU + Zr-PSU (c'') displayed significant uptake, confirming the central role of Zr-PSU in arsenic capture. The RE values reported for c'' are normalized to the Zr-PSU content, underlining the hybrid's effectiveness.

In contrast, Zr-PSU-QA displayed lower adsorption efficiency, despite the potential for ion-exchange. At alkaline pH (systems e–f, Fig. 4 blue), adsorption of As (V) sharply decreased. Under these conditions, the MOF surface becomes negatively charged ($-COO^-$), leading to strong electrostatic repulsion with AsO_4^{3-} species. As a result, only the quaternary ammonium groups contribute to uptake, though with limited efficiency. Supporting this, earlier experiments in our laboratory using PSU-QA alone (IEC = 1.6 meq/g, without MOF) yielded less than 3% RE for As (V) at pH 7, confirming the decisive role of the MOF moiety in enhancing arsenic adsorption.

For As (III) at pH 7, Zr-PSU exhibited moderate uptake, possibly facilitated by π–π surface interactions and the high porosity of the hybrid. Interestingly, at pH 12 (sample i, Fig. 4 red), Zr-PSU-QA displayed improved adsorption of As (III) compared to As (V). This can be explained by the speciation of arsenite (equilibrium between $H_2AsO_3^-$ and $HAsO_3^{2-}$), these species carry lower charge density and are less hydrated than arsenates, thereby reducing electrostatic repulsion and favoring interactions with QA-MOF active sites [44]. The smaller size and lower hydration of As (III)

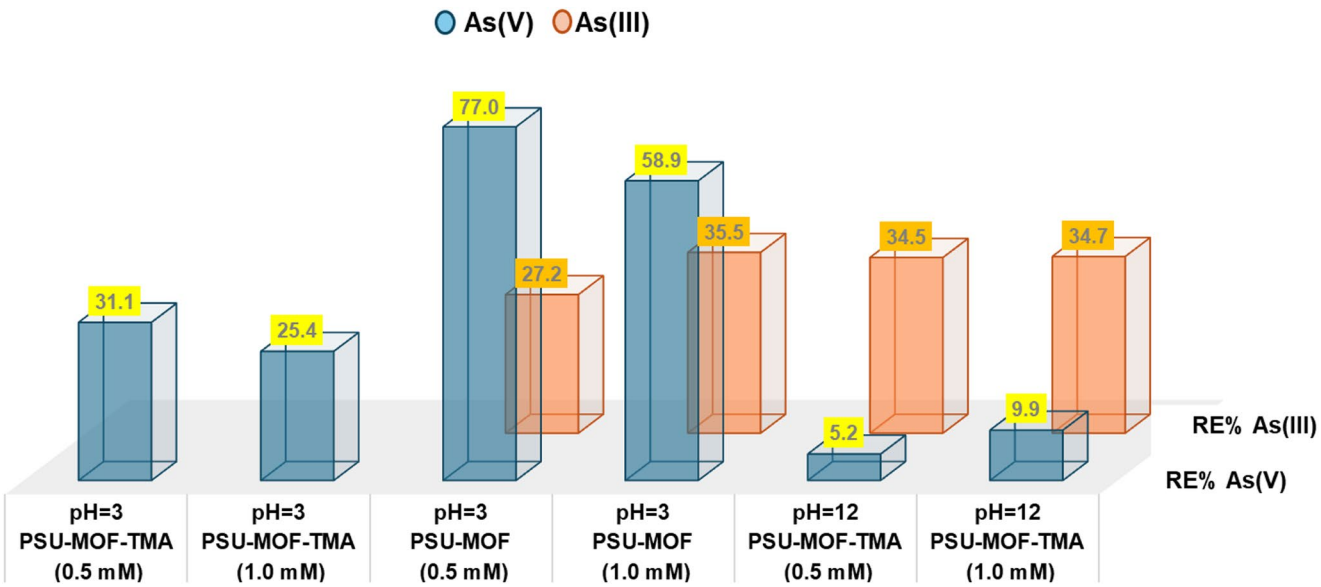

Fig. 4 Removal efficiency comparison for As(V) (blue) and As(III) (orange) in different systems and concentrations

also promote easier diffusion into the polymeric pores, unlike the bulkier, more hydrated As (V) species.

Overall, these findings highlight the importance of porosity and charge effects in governing arsenic uptake. Removal efficiency (RE%) tends to be higher at lower initial concentrations, where abundant active sites capture most arsenic ions. At higher concentrations, however, site saturation reduces RE%, while adsorption capacity (q, mg/g) increases. This trend is particularly evident under acidic conditions, for instance, sample d (1.0 mM As V, pH 3) reached RE% = 58.9 but a notably higher q ≈ 68 mg/g. Under neutral or alkaline conditions, higher concentration gradients can enhance arsenic transport to adsorption sites, partially offsetting the drop in RE.

To contextualize the performance relative to active metal loading, adsorption capacities were normalized to the bulk Zr content (63.55 ppm, determined by ICP). For the best performing sample (Zr-PSU, q_e = 43.3 mg·g^{-1}) this corresponds to 681.4 mg As per mg Zr. These large normalized values reflect the low Zr loading: adsorption is provided by the integrated MOF–polymer architecture that provides many binding sites (linker carboxyls, node hydroxyls, QA groups, and porosity), not by isolated Zr atoms alone, and emphasize the high adsorption efficiency achieved per unit metal. Notably, PSU-QA without MOF (c') exhibits only an adsorption of 2.6 mg As per mg Zr, underscoring the crucial role of the MOF-like domains in enabling effective arsenic capture.

Concerning the stability of the systems, Zr-leaching results confirm the excellent chemical robustness of both hybrid materials over a wide pH range. For Zr-PSU, zirconium release remained negligible at pH = 3 and 7 (≈0.04 ppm after 24 h), indicating strong coordination between Zr centers and the terephthalate linkers covalently anchored to the polysulfone backbone. At pH = 12, a slightly higher Zr concentration (0.51 ppm after 24 h) was observed, suggesting partial hydrolysis of peripheral Zr–O bonds in highly alkaline media. However, this still represents less than 1% of the total Zr content, demonstrating that the hybrid framework remains largely intact even under harsh conditions. The Zr-PSU-QA system displayed even lower Zr release at pH = 12 (0.084 ppm after 24 h), likely due to the presence of quaternary ammonium groups that stabilize the polymer–MOF interface and hinder Zr–O bond cleavage. The minimal leaching observed for both materials highlights the effectiveness of covalent integration in preventing detachment or dissolution of MOF-like units, an issue common in physically blended MOF/polymer composites.

To investigate the behavior of arsenic sorption process, kinetic studies were conducted on the best performing system, Zr-PSU at pH = 3 for As(V) adsorption. As shown in Fig. 5a, removal efficiency (RE%) increases with contact time, as expected. Within the first 30 min, Zr-PSU achieves 55% As (V) removal, demonstrating a rapid initial adsorption phase. Moreover, after just 8 h, the system reaches its maximum adsorption capacity for As (V). To further analyze the uptake mechanism, the adsorption kinetics were evaluated using adsorption kinetic models, the Pseudo-Second-Order (P-S-O) kinetic model. The following calculations were performed to validate the applicability of this model [45, 46].

$$\frac{dq_t}{dt} = k(q_e - q_t)^2 \tag{3}$$

$$\frac{t}{q_t} = \frac{1}{q_e^2 k} + \frac{t}{q_e} \tag{4}$$

Where q_e (mg/g) represents the amount of arsenic adsorbed onto the system at equilibrium, and q_t (mg/g) is the adsorption capacity at time t. The P-S-O kinetic model can be analyzed by plotting t/q_t versus t, where the slope of the linear fit allows for the determination of q with a value of 50 mg/g. The q_e from mass balance (43 mg/g) is slightly lower than the P-S-O model value (50 mg/g) because kinetic models provide theoretical fits, while mass balance reflects the experimental data directly [47]. The close agreement between the two values supports the reliability of the kinetic model in describing the adsorption mechanism.

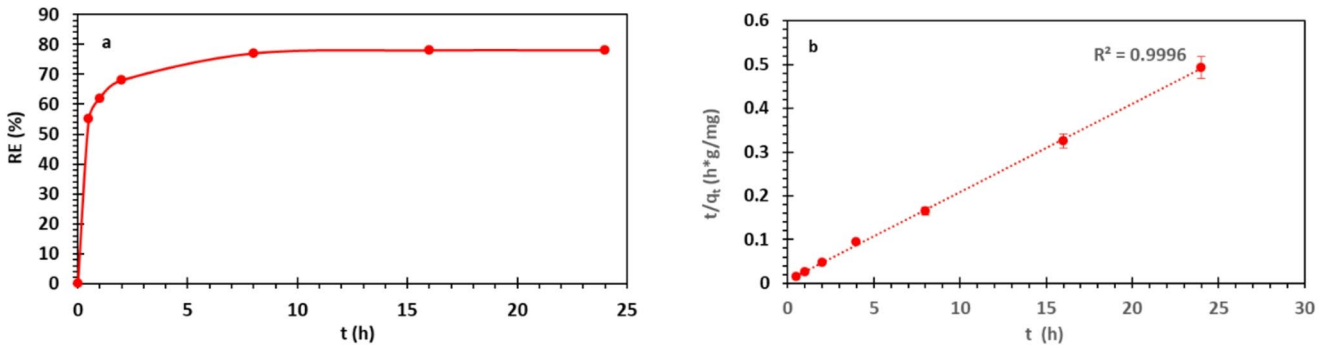

Fig. 5 **a** Removal efficiency vs. time for As(V) by Zr-PSU (pH = 3) and **b** P-S-O plot of As(V) concentration vs. time

FTIR spectra recorded after arsenic adsorption (Fig. 6) of PSU-MOF at pH = 3 show systematic, concentration-dependent shifts in several bands. The band at 857 cm^{-1} shifts to 855 and 853 cm^{-1} for 0.5 and 1.0 mM As, respectively, while the band at 660 cm^{-1} downshifts to 654 and 645 cm^{-1}, consistent with perturbation of As–O and Zr–O/Zr–OH vibrational modes. Concurrently, the feature near 818 cm^{-1} shifts upward to 829 and 833 cm^{-1} with increasing arsenic loading. The red-shifts observed for the Zr–O region indicate weakening/lengthening of Zr–O bonds upon formation of Zr–O–As inner-sphere complexes, whereas the blue-shift at 818 cm^{-1} suggests local stiffening or electronic redistribution in adjacent ligand moieties (e.g. constrained carboxylate or altered hydrogen-bonding). Collectively, these spectral changes support a dominant chemisorption mechanism involving coordination to Zr centers, accompanied by rearrangement of the neighboring polymer/MOF ligand environment. The spectrum after the regeneration of PSU-MOF at pH = 3 shows no evident differences compared to the initial spectrum under the same pH conditions (not shown).

Preliminary studies on the regeneration of Zr-PSU were conducted at pH 3 in 0.5 mM As (V). Regeneration was attempted through a simple recovery process involving immersion in a NaCl solution [48]. The regeneration efficiency was evaluated after single adsorption–desorption cycles. The system cR_3, as reported in Table 2, exhibited a regeneration efficiency of 56%, indicating only partial regeneration after the third cycle. This limited recovery suggests that the binding of $H_2AsO_4^-$ species to the Zr-PSU material is relatively strong and not easily reversed by NaCl treatment alone.

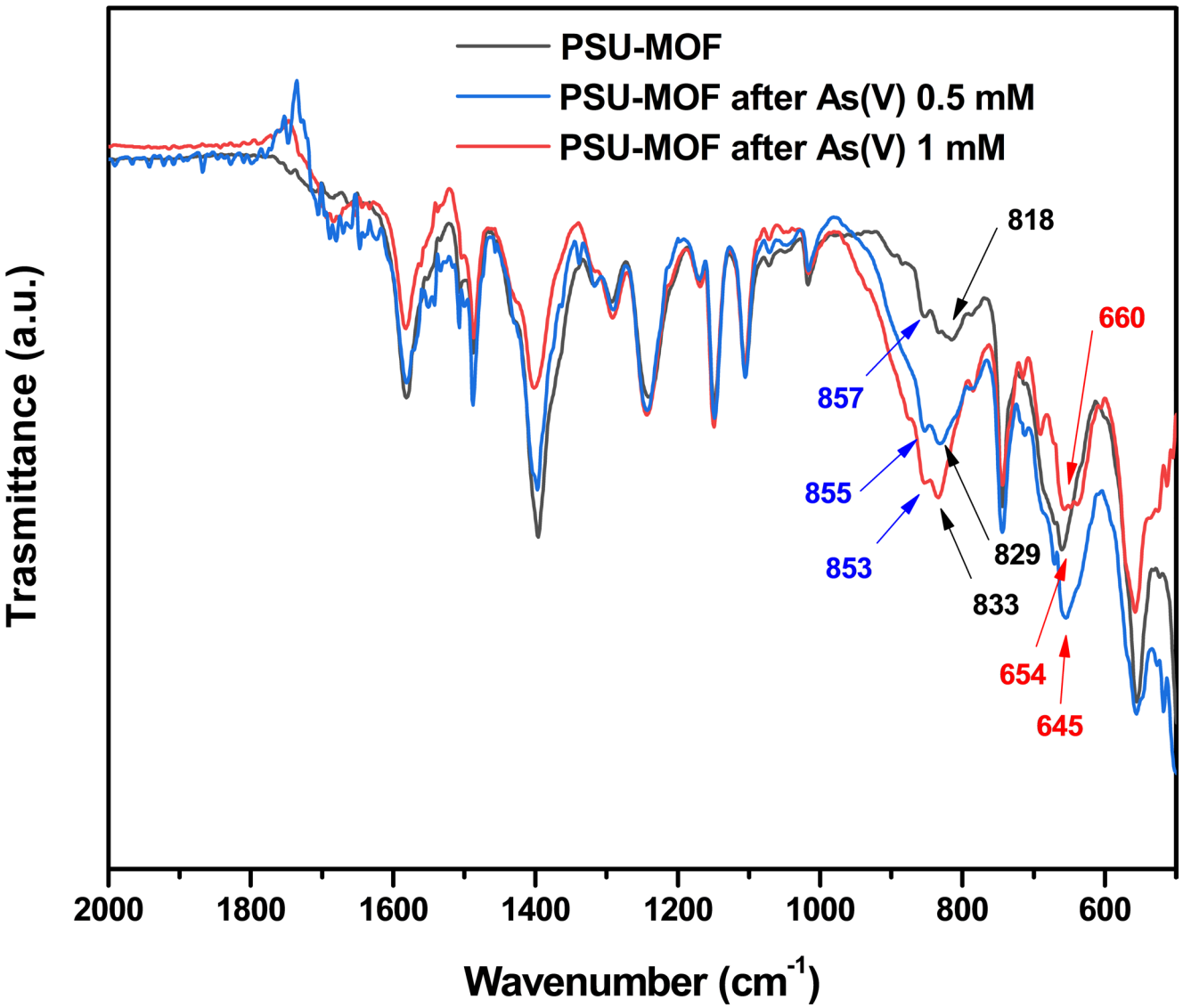

Fig. 6 FTIR spectra of Zr-PSU before and after As(V) adsorption at pH = 3 with different initial concentrations (0.5 mM and 1.0 mM)

Table 2 Regeneration of systems c (Zr-PSU) and c'' (GB/PSU + Zr-PSU) for 0.5 mM As(V) at pH = 3 after the 3rd (cR_3) and 4th ($c''R_4$) cycle respectively, and the Zr detected in solution after the regeneration

System	RE%	Regeneration efficiency%*	Zr (ppm)
c	77.0	-	
cR_3	43.0	56.0	0.037
c''	62.5	-	
$c''R_4$	61.8	98.9	0.034

* The values are calculated considering RE = 100% for the systems c and c''

The primary adsorption mechanisms likely involve coordination with hydroxyl and carboxyl functional groups on the Zr-PSU framework, forming stable inner-sphere complexes with arsenate anions. Furthermore, it is plausible that a fraction of the $H_2AsO_4^-$ species becomes immobilized within micropores, where desorption is hindered by restricted diffusion pathways and limited access to exchange sites. Consequently, chloride ions cannot fully penetrate or displace the bound arsenate species, resulting in only partial regeneration of the bulk powder. In contrast, the GB/PSU + Zr-PSU system, regenerated under identical conditions (pH = 3, 0.5 mM As(V), NaCl solution), demonstrated significantly enhanced performance. After four successive adsorption–regeneration cycles, the system maintained a regeneration efficiency of 98.9%, indicating excellent recovery and stability. This improvement is attributed to the uniform dispersion of the active material as a thin coating on the glass beads, which enhances surface accessibility and minimizes intraparticle diffusion limitations. The open structure facilitates faster ion exchange between Cl^- and adsorbed arsenate species, leading to more complete desorption and efficient regeneration. Additionally, the mechanical stability of the supported layer prevents agglomeration or structural degradation, preserving the material's long-term performance. Further studies exploring alternative regenerating agents, concentrations, and cycling conditions will help elucidate the detailed regeneration mechanism and optimize the system's reusability.

Table 3 compares various arsenic adsorption systems based on MOFs, highlighting parameters such as removal efficiency (RE%), adsorption capacity (mg/g), initial arsenic concentration, and pH. Among them, the UiO-66 system achieves a very high adsorption capacity compared to other materials. Although the removal efficiency values obtained in this work are comparable to or lower than those reported in the literature, it is important to consider the degree of functionalization of the system. Specifically, the amount of Zr-MOF-like structure is 0.3 per repeating unit of the polymer, corresponding to approximately 1.4 atomic percent of Zr. Further improvement possibilities include increasing the density of Zr-MOF-like units within the polymer matrix, to improve the adsorption capacity. Higher MOF integration could lead to a larger surface area, providing more active sites for interaction with arsenic. These strategies, by increasing the adsorption efficiency, may make Zr-PSU-based materials more competitive for water purification applications.

4 Conclusions

This study reports the application of Zr-PSU and Zr-PSU-QA systems, in which Zr–MOF-like structures are covalently linked to polysulfone, for the removal of As(III) and As(V) under different pH conditions and concentrations. The synthesis strategy was based on anchoring a terephthalate moiety onto PSU, serving as a MOF linker, followed by MOF-like assembly and quaternization. The sorption capacity of the systems was found to depend on several key factors. The charge on the MOF-like structures governed uptake in acidic conditions, while the anion-exchange mechanism in Zr-PSU-QA dominated at high pH. Porosity strongly influenced performance across all conditions. The best removal efficiency was obtained with Zr-PSU at pH 3 for As(V), while moderate As(III) uptake was observed at neutral pH. At alkaline pH, Zr-PSU-QA exhibited enhanced As(III) adsorption due to the quaternized ammonium moieties, which provide permanently positive charge sites. Adsorption kinetics followed a pseudo-second-order model, consistent with a chemisorption-driven mechanism. FTIR

Table 3 Different systems used for arsenic removal and their removal efficiency (RE%), adsorption capacity (q, mg/g), and final concentration of as (ppm)

System	RE%	q (mg/g)	[As] (ppm)	As species	pH	Refs.
PSU	20	-	1	As(V)	2.6	[49]
UiO-66	85	68.2	0.5	As(III-V)	7–10	[50]
PMS/UiO-66	95	-	1.1	As (III)	3–11	[51]
MIL-53(Fe)	99	21.3	20	As (V)	5	[52]
Fe_3O_4@UiO-66	-	73.2	150	As (V)	7	[53]
Fe–BTC	-	12.3	5	As (V)	2–12	[54]
Fe_3O_4@TA@UiO-66	80	97.8	10	As (III)	3–11	[55]
Zr-PSU	**77**	**50.0**	**62**	**As (V)**	**3**	**This work**

analysis further confirmed the adsorption mechanism, showing systematic shifts in characteristic Zr–O and aromatic vibration bands after arsenic uptake. These spectral changes indicate the formation of Zr–O–As coordination bonds, supporting a chemisorption-driven process consistent with the kinetic data. The covalent integration of MOF-like units within the polymer matrix minimized the risk of leaching or particle detachment, ensuring long-term stability and durability. This covalent design differentiates the present hybrid from conventional Zr–MOF/polymer systems, providing higher chemical stability, durability, and synergistic adsorption behavior, thus representing a significant advancement in polymer-based sorbents for water purification. Importantly, Zr leaching under highly basic conditions was found to be less than 1% of the total Zr content, confirming the robustness of the hybrid structure. Beyond their performance in batch experiments, these materials show strong potential for scalability and real-world implementation. Zr-PSU and Zr-PSU-QA can be readily processed into membranes, beads, or thin coatings without compromising structure or activity. Their excellent chemical stability across a wide pH range, minimal Zr release, and high regeneration efficiency, particularly for GB-supported systems, which maintained nearly 99% recovery after multiple cycles, highlight their suitability for reusable and environmentally sustainable water purification systems. Future optimization of MOF loading and pore structure could further enhance adsorption efficiency and selectivity.

Acknowledgements A.V. Montella thanks the PhD scholarship in Industrial Engineering for the XXXIX Cycle "Removal of pollutants in wastewater with innovative systems of composite membranes with different geometries and low environmental impact". Art. 8 D.M. n.118/2023 (Ricerca PNRR).

Author Contributions Alessio Vincenzo Montella: Investigation, Validation, Visualization, Writing - Review & Editing. Maria Bastianini: Methodology, Visualization, Investigation. Michele Sisani: Methodology, Resources. Iqbal Ahmed: investigation. Emanuela Sgreccia: Investigation. Maria Luisa Di Vona: Methodology, Resources, Writing - Review & Editing. Riccardo Narducci: Conceptualization, Methodology, Writing- Original draft preparation, Writing - Review & Editing.

Funding Open access funding provided by Università degli Studi di Roma Tor Vergata within the CRUI-CARE Agreement. This research received no external funding.

Data Availability No datasets were generated or analysed during the current study.

Declarations

Competing Interests The authors declare no competing interests.

Informed Consent Not applicable.

References

1. N. Bolan, A. Kunhikrishnan, R. Thangarajan, J. Kumpiene, J. Park, T. Makino, M.B. Kirkham, K. Scheckel, Remediation of heavy metal(loid)s contaminated soils – To mobilize or to immobilize? J. Hazard. Mater. **266**, 141–166 (2014). https://doi.org/10.1016/j.jhazmat.2013.12.018
2. Y. Ibrahim, F. Banat, V. Naddeo, S.W. Hasan, Numerical modeling of an integrated OMBR-NF hybrid system for simultaneous wastewater reclamation and Brine management. Euro-Mediterranean J. Environ. Integr. **4**(1), 23 (2019). https://doi.org/10.1007/s41207-019-0112-2
3. M. Bastianini, M. Sisani, E. Naryyev, A. Petracci, I. Di Guida, R. Narducci, Composite membranes based on Polyvinyl alcohol and lamellar solids for water decontamination. New J. Chem. **48**(5), 2128–2139 (2024). https://doi.org/10.1039/D3NJ04942F
4. Z. Maqbool, S. Hussain, M. Imran, F. Mahmood, T. Shahzad, Z. Ahmed, F. Azeem, S. Muzammil, Perspectives of using fungi as bioresource for bioremediation of pesticides in the environment: a critical review. Environ. Sci. Pollut Res. Int. **23**(17), 16904–16925 (2016). https://doi.org/10.1007/s11356-016-7003-8
5. M. Pelati, Acqua all'arsenico in 51 comuni del viterbese: il caso in Parlamento, in: Corriere (Ed.) 2021
6. T.A. Siddique, N.K. Dutta, N. Roy, Choudhury, Nanofiltration for arsenic removal: Challenges, recent Developments, and perspectives. Nanomaterials (Basel). **10**(7) (2020). https://doi.org/10.3390/nano10071323
7. X. Wang, Y. Liu, J. Zheng, Removal of As(III) and As(V) from water by Chitosan and Chitosan derivatives: a review. Environ. Sci. Pollut. Res. **23**(14), 13789–13801 (2016). https://doi.org/10.1007/s11356-016-6602-8
8. L. Yang, S. Kinoshita, T. Yamada, S. Kanda, H. Kitagawa, M. Tokunaga, T. Ishimoto, T. Ogura, R. Nagumo, A. Miyamoto, M. Koyama, A metal-organic framework as an electrocatalyst for ethanol oxidation. Angew Chem. Int. Ed. Engl. **49**(31), 5348–5351 (2010). https://doi.org/10.1002/anie.201000863
9. G. Song, Z. Wang, L. Wang, G. Li, M. Huang, F. Yin, Preparation of MOF(Fe) and its catalytic activity for oxygen reduction reaction in an alkaline electrolyte. Chin. J. Catal. **35**(2), 185–195 (2014). https://doi.org/10.1016/S1872-2067(12)60729-3
10. J. Mao, L. Yang, P. Yu, X. Wei, L. Mao, Electrocatalytic four-electron reduction of oxygen with copper (II)-based metal-organic frameworks. Electrochem. Commun. **19**, 29–31 (2012). https://doi.org/10.1016/j.elecom.2012.02.025
11. H.J. Kim, K. Talukdar, S.-J. Choi, Tuning of Nafion® by HKUST-1 as coordination network to enhance proton conductivity for fuel cell applications. J. Nanopart. Res. **18**(2), 47 (2016). https://doi.org/10.1007/s11051-016-3346-9
12. H.A. Patel, N. Mansor, S. Gadipelli, D.J. Brett, Z. Guo, Superacidity in Nafion/MOF hybrid membranes retains water at low

humidity to enhance proton conduction for fuel cells. ACS Appl. Mater. Interfaces. **8**(45), 30687–30691 (2016). https://doi.org/10.1021/acsami.6b12240
13. A. Donnadio, R. Narducci, M. Casciola, F. Marmottini, R. D'Amato, M. Jazestani, H. Chiniforoshan, F. Costantino, Mixed membrane matrices based on Nafion/UiO-66/SO3H-UiO-66 Nano-MOFs: revealing the effect of crystal Size, Sulfonation, and filler loading on the mechanical and conductivity properties. ACS Appl. Mater. Interfaces. **9**(48), 42239–42246 (2017). https://doi.org/10.1021/acsami.7b14847
14. J. Escorihuela, R. Narducci, V. Compañ, F. Costantino, Proton conductivity of composite polyelectrolyte membranes with Metal-Organic frameworks for fuel cell applications. Adv. Mater. Interfaces. **6**(2), 1801146 (2019). https://doi.org/10.1002/admi.201801146
15. H. Kaur, N. Devi, S.S. Siwal, W.F. Alsanie, M.K. Thakur, V.K. Thakur, Metal–Organic Framework-Based materials for wastewater treatment: superior adsorbent materials for the removal of hazardous pollutants. ACS Omega. **8**(10), 9004–9030 (2023). https://doi.org/10.1021/acsomega.2c07719
16. H. Molavi, Cerium-based metal-organic frameworks: Synthesis, properties, and applications. Coord. Chem. Rev. **527**, 216405 (2025). https://doi.org/10.1016/j.ccr.2024.216405
17. X. Liu, Y. Shan, S. Zhang, Q. Kong, H. Pang, Application of metal organic framework in wastewater treatment. Green. Energy Environ. **8**(3), 698–721 (2023). https://doi.org/10.1016/j.gee.2022.03.005
18. F. Ahmadijokani, H. Molavi, M. Rezakazemi, S. Tajahmadi, A. Bahi, F. Ko, T.M. Aminabhavi, J.-R. Li, M. Arjmand, UiO-66 metal–organic frameworks in water treatment: A critical review. Prog. Mater. Sci. **125**, 100904 (2022). https://doi.org/10.1016/j.pmatsci.2021.100904
19. Y.-H. Li, C.-C. Wang, X.-H. Yi, H.-Y. Chu, UiO-66(Zr)-based functional materials for water purification: an updated review. Environ. Funct. Mater. **2**(2), 93–132 (2023). https://doi.org/10.1016/j.efmat.2024.02.001
20. K. Ahmad, M.A. Nazir, A.K. Qureshi, E. Hussain, T. Najam, M.S. Javed, S.S.A. Shah, M.K. Tufail, S. Hussain, N.A. Khan, H.--R. Shah, M. Ashfaq, Engineering of zirconium based metal-organic frameworks (Zr-MOFs) as efficient adsorbents. Mater. Sci. Engineering: B **262**, 114766 (2020). https://doi.org/10.1016/j.mseb.2020.114766
21. C. Wang, X. Liu, J.P. Chen, K. Li, Superior removal of arsenic from water with zirconium metal-organic framework UiO-66. Sci. Rep. **5**(1), 16613 (2015). https://doi.org/10.1038/srep16613
22. L. Feng, K.-Y. Wang, G.S. Day, M.R. Ryder, H.-C. Zhou, Destruction of Metal–Organic frameworks: positive and negative aspects of stability and lability. Chem. Rev. **120**(23), 13087–13133 (2020). https://doi.org/10.1021/acs.chemrev.0c00722
23. S. Rajeev, U.G. Panicker, P.-M.O. Frameworks, Recent advances in synthesis strategies and applications. J. Inorg. Organomet. Polym Mater. **35**(7), 5157–5188 (2025). https://doi.org/10.1007/s10904-025-03616-8
24. N. Naz, M.H. Manzoor, S.M.G. Naqvi, U. Ehsan, M. Aslam, F. Verpoort, Porous organic polymers; an emerging material applied in energy, environmental and biomedical applications. Appl. Mater. Today. **38**, 102198 (2024). https://doi.org/10.1016/j.apmt.2024.102198
25. M.G. Mohamed, A.F.M. El-Mahdy, M.G. Kotp, S.-W. Kuo, Advances in porous organic polymers: syntheses, structures, and diverse applications. Mater. Adv. **3**(2), 707–733 (2022). https://doi.org/10.1039/D1MA00771H
26. J. Lee, J. Lee, J.Y. Kim, M. Kim, Covalent connections between metal–organic frameworks and polymers including covalent organic frameworks. Chem. Soc. Rev. **52**(18), 6379–6416 (2023). https://doi.org/10.1039/D3CS00302G
27. Z. Zhang, H.T. Nguyen, S.A. Miller, S.M. Cohen, PolyMOFs: A class of interconvertible Polymer-Metal-Organic-Framework hybrid materials. Angew Chem. Int. Ed. Engl. **54**(21), 6152–6157 (2015). https://doi.org/10.1002/anie.201502733
28. S. Ayala, Z. Zhang, S.M. Cohen, Hierarchical structure and porosity in UiO-66 PolyMOFs. Chem. Commun. **53**(21), 3058–3061 (2017). https://doi.org/10.1039/C6CC10225E
29. R. Lin, L. Ge, L. Hou, E. Strounina, V. Rudolph, Z. Zhu, Mixed matrix membranes with strengthened MOFs/Polymer interfacial interaction and improved membrane performance. ACS Appl. Mater. Interfaces. **6**(8), 5609–5618 (2014). https://doi.org/10.1021/am500081e
30. N. Tien-Binh, D. Rodrigue, S. Kaliaguine, In-situ cross interface linking of PIM-1 polymer and UiO-66-NH2 for outstanding gas separation and physical aging control. J. Membr. Sci. **548**, 429–438 (2018). https://doi.org/10.1016/j.memsci.2017.11.054
31. K. Xie, Q. Fu, Y. He, J. Kim, S.J. Goh, E. Nam, G.G. Qiao, P.A. Webley, Synthesis of well dispersed polymer grafted metal–organic framework nanoparticles. Chem. Commun. **51**(85), 15566–15569 (2015). https://doi.org/10.1039/C5CC06694H
32. W. Zhou, Y. Liu, W.L. Teo, B. Chen, F. Jin, L. Zhang, Y. Zeng, Y. Zhao, Construction of a sandwiched MOF@COF composite as a Size-Selective catalyst. Cell. Rep. Phys. Sci. **1**(12), 100272 (2020). https://doi.org/10.1016/j.xcrp.2020.100272
33. R. Narducci, E. Sgreccia, A.V. Montella, G. Ercolani, S. Kaciulis, S. Syahputra, E. Bloch, L. Pasquini, P. Knauth, M.L. Di Vona, One-Component catalytic electrodes from Metal–Organic frameworks covalently linked to an anion exchange ionomer. Molecules. **30**(6), 1230 (2025). https://doi.org/10.3390/molecules30061230
34. M.L. Di Vona, M. Casciola, A. Donnadio, M. Nocchetti, L. Pasquini, R. Narducci, P. Knauth, Anionic conducting composite membranes based on aromatic polymer and layered double hydroxides. Int. J. Hydrog. Energy. **42**(5), 3197–3205 (2017). https://doi.org/10.1016/j.ijhydene.2016.11.030
35. L. Vaccaro, A. Marrocchi, V. Trombettoni, R. Narducci, M.L. Di Vona, continuous flow production of ion exchange membranes immobilized on glass support, WO2022144718A1
36. B.C. Smith, T.C. Group, V. Part, Carboxylates—Coming Clean. Spectrosc. **33**(5), 20–23 (2018)
37. J. Pascual-Colino, B. Artetxe, G. Beobide, O. Castillo, M.L. Fidalgo-Mayo, A. Isla-López, A. Luque, S. Mena-Gutiérrez, S. Pérez-Yáñez, The chemistry of Zirconium/Carboxylate clustering process: acidic conditions to promote Carboxylate-Unsaturated octahedral hexamers and pentanuclear species. Lnorg Chem. **61**(12), 4842–4851 (2022). https://doi.org/10.1021/acs.inorgchem.1c03466
38. J. Zhou, M. Unlu, J.A. Vega, P.A. Kohl, Anionic polysulfone ionomers and membranes containing fluorenyl groups for anionic fuel cells. J. Power Sources. **190**(2), 285–292 (2009). https://doi.org/10.1016/j.jpowsour.2008.12.127
39. Y. Yu, L. Yu, K. Shih, J.P. Chen, Yttrium-doped iron oxide magnetic adsorbent for enhancement in arsenic removal and ease in separation after applications. J. Colloid Interface Sci. **521**, 252–260 (2018). https://doi.org/10.1016/j.jcis.2018.02.046
40. T.T. Pham, H.H. Ngo, V.S. Tran, M.K. Nguyen, Removal of as (V) from the aqueous solution by a modified granular ferric hydroxide adsorbent. Sci. Total Environ. **706**, 135947 (2020). https://doi.org/10.1016/j.scitotenv.2019.135947
41. M. Chiban, M. Zerbet, G. Cârjă, F. Sinan, Application of low-cost adsorbents for arsenic removal: A review, 2012. 0.5897/JECE11.013
42. M.R. Azhar, H.R. Abid, V. Periasamy, H. Sun, M.O. Tade, S. Wang, Adsorptive removal of antibiotic sulfonamide by UiO-66 and ZIF-67 for wastewater treatment. J. Colloid Interface Sci. **500**, 88–95 (2017). https://doi.org/10.1016/j.jcis.2017.04.001

43. T. Virtanen, G. Rudolph, A. Lopatina, B. Al-Rudainy, H. Schagerlöf, L. Puro, M. Kallioinen, F. Lipnizki, Analysis of membrane fouling by Brunauer-Emmet-Teller nitrogen adsorption/desorption technique. Sci. Rep. **10**(1) (2020). https://doi.org/10.1038/s41598-020-59994-1
44. X. Zhang, Q. Dong, Y. Wang, Z. Zhu, Z. Guo, J. Li, Y. Lv, Y.T. Chow, X. Wang, L. Zhu, G. Zhang, D. Xu, Water-stable metal–organic framework (UiO-66) supported on zirconia nanofibers membrane for the dynamic removal of Tetracycline and arsenic from water. Appl. Surf. Sci. **596**, 153559 (2022). https://doi.org/10.1016/j.apsusc.2022.153559
45. M. Samimi, M. Zakeri, F. Alobaid, B. Aghel, A brief review of recent results in arsenic adsorption process from aquatic environments by Metal-Organic frameworks: classification based on kinetics. Isotherms Thermodyn. Behav. Nanomaterials. **13**(1), 60 (2023). https://doi.org/10.3390/nano13010060
46. E. Sgreccia, C. Rogalska, F.S. Gallardo Gonzalez, P. Prosposito, L. Burratti, P. Knauth, M.L. Di Vona, Heavy metal decontamination by ion exchange polymers for water purification: counterintuitive cation removal by an anion exchange polymer. J. Mater. Sci. **59**(7), 2776–2787 (2024). https://doi.org/10.1007/s10853-024-09356-3
47. E.D. Revellame, D.L. Fortela, W. Sharp, R. Hernandez, M.E. Zappi, Adsorption kinetic modeling using pseudo-first order and pseudo-second order rate laws: A review. Clean. Eng. Technol. **1**, 100032 (2020). https://doi.org/10.1016/j.clet.2020.100032
48. E. Sgreccia, F.S. Gallardo Gonzalez, P. Prosposito, L. Burratti, M. Sisani, M. Bastianini, P. Knauth, M.L. Di Vona, Heavy Metal Detection and Removal by Composite Carbon Quantum Dots/Ionomer Membranes, Membranes 14(6), 134 (2024). https://doi.org/10.3390/membranes14060134
49. S. Gupta, D. Bhatiya, C.N. Murthy, Metal removal studies by composite membrane of polysulfone and functionalized Single-Walled carbon nanotubes. Sep. Sci. Technol. **50**(3), 421–429 (2015). https://doi.org/10.1080/01496395.2014.973516
50. X. He, F. Deng, T. Shen, L. Yang, D. Chen, J. Luo, X. Luo, X. Min, F. Wang, Exceptional adsorption of arsenic by zirconium metal-organic frameworks: engineering exploration and mechanism insight. J. Colloid Interface Sci. **539**, 223–234 (2019). https://doi.org/10.1016/j.jcis.2018.12.065
51. Z. Xie, Q. He, S. Liu, X. Huang, M. Dai, Q. Chen, A. Sun, J. Ye, X. Tan, W. Xu, Enhanced removal of As(iii) by manganese-doped defective UiO-66 coupled peroxymonosulfate: multiple reactive oxygen species and system stability. Environ. Science: Nano. **11**(8), 3585–3598 (2024). https://doi.org/10.1039/D4EN00194J
52. T.A. Vu, G.H. Le, C.D. Dao, L.Q. Dang, K.T. Nguyen, Q.K. Nguyen, P.T. Dang, H.T.K. Tran, Q.T. Duong, T.V. Nguyen, G.D. Lee, Arsenic removal from aqueous solutions by adsorption using novel MIL-53(Fe) as a highly efficient adsorbent. RSC Adv. **5**(7), 5261–5268 (2015). https://doi.org/10.1039/C4RA12326C
53. J.-B. Huo, L. Xu, X. Chen, Y. Zhang, J.-C.E. Yang, B. Yuan, M.-L. Fu, Direct epitaxial synthesis of magnetic Fe3O4@UiO-66 composite for efficient removal of arsenate from water. Microporous Mesoporous Mater. **276**, 68–75 (2019). https://doi.org/10.1016/j.micromeso.2018.09.017
54. B.-J. Zhu, X.-Y. Yu, Y. Jia, F.-M. Peng, B. Sun, M.-Y. Zhang, T. Luo, J.-H. Liu, X.-J. Huang, Iron and 1,3,5-Benzenetricarboxylic Metal–Organic coordination polymers prepared by solvothermal method and their application in efficient As(V) removal from aqueous solutions. J. Phys. Chem. C **116**(15), 8601–8607 (2012). https://doi.org/10.1021/jp212514a
55. P. Qi, R. Luo, T. Pichler, J. Zeng, Y. Wang, Y. Fan, K. Sui, Development of a magnetic core-shell Fe3O4@TA@UiO-66 microsphere for removal of arsenic(III) and antimony(III) from aqueous solution. J. Hazard. Mater. **378**, 120721 (2019). https://doi.org/10.1016/j.jhazmat.2019.05.114